Article

Journal of Nanoscience and Nanotechnology
Vol. 18, 3713–3721, 2018
www.aspbs.com/jnn

Influence of Thermal Modification and Morphology of TiO_2 Nanotubes on Their Electrochemical Properties for Biosensors Applications

Katarzyna Arkusz*, Ewa Paradowska, Marta Nycz, and Elżbieta Krasicka-Cydzik

Department of Mechanical Engineering, University of Zielona Gora, ul.Licealna 9, 65-417 Zielona Gora, Poland

The morphology of self-assembled TiO_2 nanotubes layer plays a key role in electrical conductivity and biocompatibility properties in terms of cell proliferation, adhesion and mineralization. Many research studies have been reported in using a TiO_2 nanotubes for different medical applications, there is a lack of unified correlation between TNT morphology and its electrochemical properties. The aim of this study was to examine the effects of diameter and annealing conditions on TiO_2 nanotubes with identical height and their behaviour as biosensor platform. TiO_2 nanotubes layer, 1000 nm thick with nanotubes of diameters in range: $25 \div 100$ nm, was prepared by anodizing of the titanium foil in ethylene glycol solution. To change the crystal structure and improve the electrical conductivity of the semiconductive TiO_2 nanotubes layer the thermal treatment by annealing in argon, nitrogen or air was used. Basing on the electrochemical tests, the XPS and scanning microscopy examinations, as well as the contact angle measurements and the amperometric detection of potassium ferricyanide, it was concluded that the 1000 nm thick TiO_2 nanotubes layer with nanotubes of 50 nm diameter, annealed in argon, showed the best physicochemical properties, which helps investigate the adsorption immobilization mechanism. The possibility of using TNT as a biosensor platform was confirmed in hydrogen detection.

Keywords: TiO_2 Nanotubes (TNT), Biosensing, Thermal Modification.

1. INTRODUCTION

Biosensors market is the fastest growing segment among modern analytical methods used in the fields of medicine, biotechnology, agriculture, environment and food industry.[1] Numerous studies related to the development of new biosensors focus on maintaining the highest limit of detection. New composite material or highly sensitive detection method (i.e., micro Raman spectroscopy, laser techniques) are used for this purpose. Recently, the most popular biosensor platform are nanocomposites containing graphene and metal nanoparticles,[2–4] carbon glassy and carbon nanotubes[5–7] or more complicated ones.[8] As defined by biosensor definition, material used as a biosensor platform need to be cheap, disposable and environmentally-friendly.

Numerous studies[9–15] have confirmed that titanium oxide nanotubes (TNT) are one of the most promising candidate materials for fabrication of biosensors and implantable biodevices. Favorable adsorption, electrical conductance, large surface-to-volume ratio, porosity, high homogeneity and free energy, ability to bind protein make the TNT layer a good platform to electrochemical biosensor.[16] Although titanium oxide nanotubes (TNT) have been used as a biosensor platform, the geometric effects of the nanotubes on chemical compounds and protein adhesion are still an open discussion.[17–21]

Controlled morphology for TNT layer plays a key role in biomedical application. Many factors affect the morphology of TNT formed by anodization process, such as applied voltage, anodizing time, electrolyte composition, pH and temperature. The influence of each anodizing parameters on morphology of TNT was analyzed in the literature. It was demonstrated that TNT diameter depends on anodizing potential[22,23] and on pH values of electrolyte.[24,25] Time of anodizing process,[26] kind of electrolyte and its pH[25–27] influence the thickness of TNT. Type of electrolyte also incluences the shape of TiO_2 nanotubes—TNT formed in inorganic electrolyte has a barrel shape and its high does not exceed 500 nm.[28,29]

*Author to whom correspondence should be addressed.

TNT formed in organic electrolyte has a regular form and smooth wall.[30]

Recent studies allow to determine the general correlations between anodizing parameters and TNT morphology. A multitude of parameters affecting the structure of TNT cause considerable difficulties in defining the anodizing conditions essential for producing the TNT layers with specified morphology precisely. Although TNT nanotubes were first made in 1991,[31] research on determining the relationship between all the above mentioned parameters, and the morphology of nanostructures, is still ongoing.[26, 32] General rules on how the anodizing parameters influence morphological parameters of obtained TNT attempted to determine its electrochemical, electrical[33] and photocatalytic[34] properties. Giorgi et al.[33] carried out a measurement, the aim of which was to determine the conductive properties of electrochemical TNT. They took into account only one sample of nanotubes with a diameter of 58 nm and height of 10 μm. The nanotubes were also annealed and then the ohmic resistance, electron diffusion coefficient and lifetime was set. No changes of electric properties of TNT according to its morphology were analyzed.

The influence of morphological parameters on the photocatalytic properties of TNT was determined by Adan et al.[34] Only potential changes were considered during anodizing process thereby the obtained TNT have both different diameters and different heights. Attempts to determine the effect of morphological parameters on physico-chemical properties of TNT made so far, were performed only on the structures differed by more than one factor. The diameter of nanostructured TiO_2 plays the key role in biomedical application of TNT,[14–21, 35] i.e., drug delivering, cell adhesion, biosensing. Current research on the influence of morphological parameter on immobilization efficiency on TNT surface indicates the favourable ability to protein binding on TNT with diameter less than 50 nm.[15] Similar conclusions were obtained by Gongadze[14, 36] in studies on behaviour of osteoblast in contact with TNT layer. Analysis of mesenhymall cell adhesion on TNT[19] indicates improve cell activity on TNT layer with diameter of 15–30 nm. Cell proliferation increased with the TNT diameter decreasing.[37] Diameter of TNT were studied to analyse the alkaline phosphate, colagen-I gene expression.[38] Increasing gene expression were prove on TNT with 70 nm diameter, which confirms the possibility of orthopedic implants modulation through a layer of TNT. Antibacterial properties of TNT were show in experiment[39–41] for layer characterized by 50 nm diameter and 200 nm high. Obtained results in described measurements have not been confirmed by electrochemical analysis yet.

In order to improve the adsorption and electrochemical properties of TNT, the thermal treatments are frequently used. Many research on determining the temperature, time and atmosphere of annealing were carried out.[42–55] Annealing of TiO_2 nanotubes having mixed crystal structure (anatase, rutile) are excellent semiconductors and can be used as biosensor electrode. Only Alhosan[42] performed a study on the electrochemical characteristics of TNT having a diameter of 80 nm and a height of 380 nm before and after annealing in air, nitrogen and carbon dioxide. It was shown that TNT electrical conductivity is increased in the presence of TiO_2 in the anatase form. There were no specific research to determine the effect of annealing atmosphere on the physicochemical properties of structures TNT.

In summary, numerous research work have determined the physical and chemical properties of TNT. They most accurately describe only the formation mechanism of TNT with regard to the influence of anodizing parameters on TNT morphology. Attempts to characterize the TNT have been taken, however analyzed TNT have both different diameters and different heights, which results in incorrect or imprecise conclusions owing to different surface tension, porosity etc. Accordingly, the aim of our work is to evaluate solaly the effect of diameter of TiO_2 nanotubes and thermal treatment condition on their physicochemical and adsorption properties. Analyzed TNT are of equal hight, what has not been considered in literature. The investigation helps to understand the physisorption mechanism of chemical compound, used as a biological substance model onto TNT film. In this work, the synthesis of titanium oxide nanotubes with a diameter range $25 \div 100$ nm by electrochemical anodizing and the comparison of their physicochemical and adsorption properties are described. The effect of the thermal modification of TNT by annealing in argon, nitrogen or air atmosphere on the ability of protein binding on the conductivity is investigated. The potassium ferricyanide detection is chosen as a preleminary model reaction. The optimized titanium nanotube structures for biosensors applications were confirmed in hydrogen peroxide detection.

2. EXPERIMENTAL DETAILS

2.1. Materials

Titanium foil (99.9% purity), ethylene glycol (assay 99.8%), ammonium fluoride NH_4F, potassium ferricyanide $K_3[Fe(CN)_6]$, Horseradish peroxidase (HRP) and hydrogen dioxide (H_2O_2) were purchased from Sigma-Aldrich (UK) and used as supplied. Phosphate buffered saline (PBS, 0.01 M, pH 7.4) was employed as supporting electrolyte for all electrochemical experiments. All solution were prepared from high purity reagents and distilled water.

2.2. Methods

2.2.1. TiO_2 Nanotubes Fabrication

The titanium foil was sonicated in acetone, ethanol and distilled water and dried in nitrogen. The formation of

Table I. Parameters of TNT formation with diameter (ϕ): 25, 50, 75, 100 nm and 1000 nm thickness.

TNT	$\phi = 25$ nm	$\phi = 50$ nm	$\phi = 75$ nm	$\phi = 100$ nm
Concentration of $C_2H_6O_2$ [%]	90	85	90	85
Potential [V]	10	17	30	40
Anodizing time [s]	600	3750	900	1100

nanotube oxide layers was performed by electrochemical anodizing in various concentrations of ethylene glycol solution with 0.65% wt. NH_4F. The formation process consists of two stages: the first potentiodynamic and the second potentiostatic. At the beginning the foil was polarized up to the set potential with scan rate 0.5 V/s and then was kept at the set potential for further anodizing time in the same electrolyte. 1000 ± 100 nm thick surface layers of vertically arranged titania nanotubes of diameter range $25 \div 100 \pm 5$ nm were obtained according to anodizing parameters (Table I). Field emission scanning electron microscopy (FESEM, JEOL JSM-7600F) and energy-dispersive X-ray spectroscopy (EDS, Oxford INCA) were used to investigate surface morphology and chemical composition.

2.2.2. Thermal Modification

The obtained TNT layers were annealed in argon, nitrogen or air at 550 °C for 2 hours with the heating rate of 30 °C/min to the desired annealing temperature. Field emission scanning electron microscopy (FESEM, JEOL JSM-7600F) and energy-dispersive X-ray spectroscopy (EDS, Oxford INCA) were used to investigate surface morphology and chemical composition.

XPS spectra were recorded using the X-ray Photoelectron Spectroscopy (XPS) in a equipment by VSW (Vacuum Systems Workshop, Ltd.) equipped with a concentric hemispherical electron analyzer with radius of 150 mm and two-plate 18-channel detector (Galileo). The electron analyzer was operated in fixed-analyse transmission mode with constant pass energy of 22.5 eV. Samples were exposed to the Kα Mg (1253.6 eV) X-ray radiaton. The background pressure during the analyses was greater than 5×10^{-8} mbar. To check the reproducibility of the results, survey spectra and high resolution spectra for Ti 2p and O 1s were recorded on two different locations on each specimen.

2.2.3. Electrochemical Measurements

Open circuit potential (OCP) of Ti/TNT measurements were carried out at room temperature for 1800 s. Electrochemical impedance spectroscopy (EIS) spectra were performed over a frequency range of 10^5–0.1 Hz with an acquisition of 10 points per decade and with a signal amplitude of 10 mV. Cyclic voltammetry tests (CV) for every samples were carried out in PBS (0.01 M, 10 ml, pH 7.4) for potential ranging from $-1 \div 1$ V versus Ag/AgCl with scan rate 0.05 V/s.

HRP alone or with Th were immobilized on the surface of prepared electrodes using dip coating methods for 48 h. The 0.01 mM H_2O_2 solution was added to PBS electrolyte to detect its electrochemically.

A potentiostat/galvanostat model PGSTAT-302N from AutoLab (EcoChemie, Utrecht, The Netherlands) was used to perform these experiments. All measurements were performed in the standard three-electrode configuration with Ti/TNT electrode as the working electrode, the standard silver chloride electrode ($E_{Ag/AgCl} = 0.222$ V) as the reference electrode and a platinum foil as the auxiliary electrode in PBS (0.01 M, pH 7.4) solution at 25 ± 2 °C.

2.2.4. Contact Angle Measurements

Dynamic contact angle measurements were performed using distilled water at room temperature using PG-3 Goniometer equipped with a microscope, a camera and an integrated micro-pump, which deliver accurate droplets in 0.5 μl steps.

3. RESULTS AND DISCUSSION

3.1. Characterization of Non-Anodized TNT

Figure 1 shows the FE-SEM micrographs of TiO_2 nanotubes, 1000 ± 100 nm thick with varying diameters before thermal treatment. The images show highly ordered, vertically aligned nanotubes with four average internal diameters between 25 ± 5 and 100 ± 5 nm, created by controlling potentials ranging from 10 to 40 V, anodized in ethylene glycol solution with 0.65 wt.% NH_4F, as previously reported.[32] These images demonstrate diameters of TiO_2 nanotubes increase as the anodization voltage is

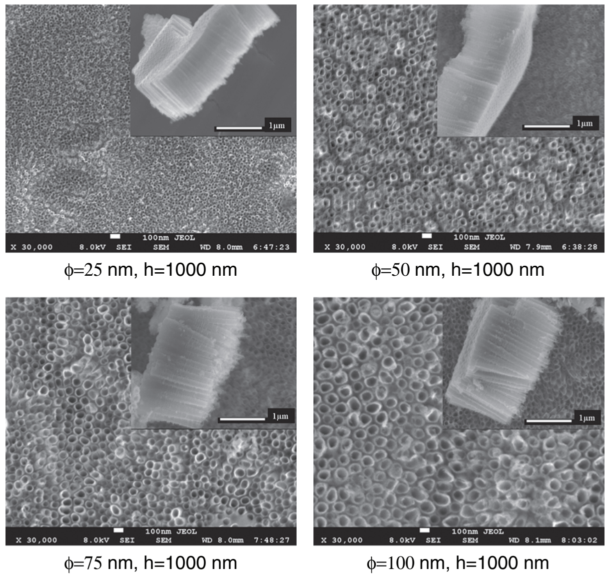

Figure 1. SEM top-view and cross-sectional images of TNT layers, 1000 nm thick (h) with nanotubes of diameters (ϕ): 25, 50, 75, 100 nm.

Table II. Water contact angle (WCA) and open circuit potential (OCP) measurements of TNT layers, 1000 nm thick (h) with nanotubes of diameters (ϕ): 25, 50, 75, 100 nm.

TNT	WCA [°]	OCP [mV] versus Ag/AgCl
$\phi = 25$ nm, $h = 1000$ nm	$15 \pm 4°$	-224 ± 10
$\phi = 50$ nm, $h = 1000$ nm	$20 \pm 2°$	-220 ± 10
$\phi = 75$ nm, $h = 1000$ nm	$24 \pm 3°$	-200 ± 10
$\phi = 100$ nm, $h = 1000$ nm	$<90°$	-162 ± 10

increased. TNT formed in organic solution have smooth walls without any perforation.

The water contact angle (WCA) measurements of TNT are listed in Table II. This results show that morphology of nanotubes affect the surface hydrophilicity. It was impossible to measure the WCA of 100 nm diameter TNT, because imposed drop on the surface was melted and rapidly absorbed. It was assumed that the contact angle is less than 90°. However, the water contact angle of non-anodized TNT with pore size smaller than 75 nm increases with the increase of value of pore size, ranging from 17 to 24 °C. The uncertainty of measurement in the total area of the TNT is the reason for this dependency. TNT surface changes influence the surface free energy and dynamic wettability. It means that nanotubular titanium dioxide layer having a diameter of nanotubes close to 1 nm represent complete wetting. Obtained results differ from others described in the literature.[30,56] Yoriya et al. analyzed the wettability of TNT anodized in varying potential without retaining the same thickness of TNT layer. Increased diameters of TNT caused the decreasing of the layer thickness, so the porosity of TNT should be also analyzed. In our measurement only effect of nanotubes diameter was analyzed. WCA values published by other authors[57] represent similar dependency but are higher than obtained in this work because of the time measurements. It is also observed that shorter time of WCA measurement indicates higher values of TNT contact angle.

Table II also shows also the open circuit potential (OCP) values for non-annealed samples of TiO_2 nanotubes with varying diameter measured in PBS solution at room temperature, during 1800 s. Increasing the diameter of TiO_2 nanotube correlates with the value of OCP increased. It also correlates with the water contact angle values. Increased hydrophilicity of TNT reduces time to determine the potential stationary. This correlation was not observed in Liu measurements[58] on OPC potential of TNT with varying diameter measured in artificial saliva. The reason is both different wall thickness and the thickness of TNT layer. Similar values of OCP recorded for TNT with diameter 25 and 50 nm confirm the results showing that the nanotubes had higher OCP especially the 30 nm diameter nanotubes.[59]

The EIS measurements of the non-annealed TiO_2 nanotubes with varying diameter are shown in Figure 2 in Bode and Nyquist representations. The Nyquist diagrams

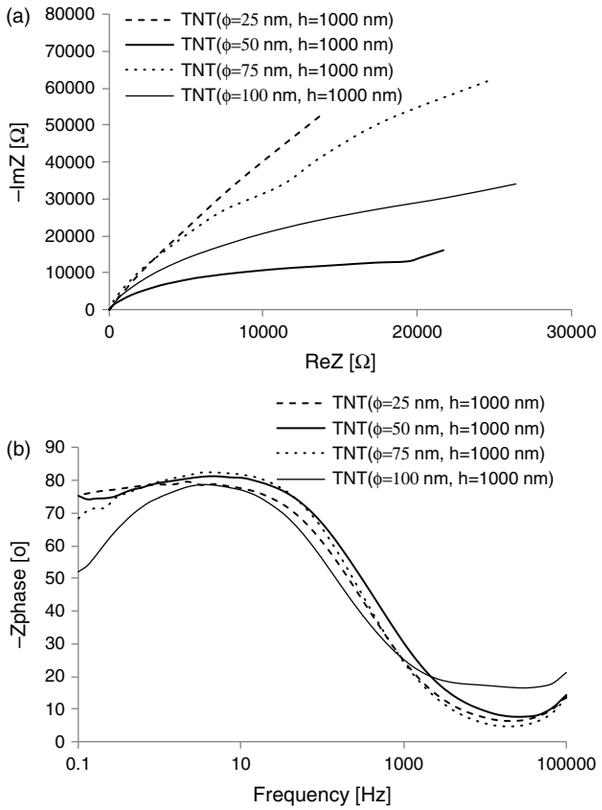

Figure 2. Nyquist (a) and Bode (b) plots of various diameters of TNT (ϕ): 25, 50, 75, 100 nm and 1000 nm thick. Spectra were recorded in the PBS solution (0.01 M, 10 ml, pH 7.4) over the frequency range 0.1–10^5 Hz with amplitude 10 mV versus $E_{Ag/AgCl} = 0.222$ V.

in Figure 2(a), determined for various diameters of the TNT nanotubes present fragments of large, incomplete semicircles, typical impedance response of thin oxide layers. It can be seen that the resistance of TNT layer depends on the diameter of the TiO_2 nanotubes. The increase in TNT layer resistance depends on the increase of TiO_2 nanotubes diameter. TNT layer with a diameter of 50 nm and 1000 nm exhibits the highest resistive character, which indicates its electrical conductivity better than the other samples. Maximum values of phase angles presented in Bode diagrams (Fig. 2(b)), recorded in the lowest frequencies (0.1 Hz) are similar and in range $50 \div 80°$. The phase angle values is related to the porosity of sample surface. Bode curves confirmed that the increase of TNT diameter characterized the increased porosity of the analyzed nanostructure. The impedance spectras recorded for all test samples have one time constant with frequency about 10 Hz, which confirms the presence of an oxide layer on the Ti film.

Figure 3(a) shows the cyclic voltammogram of non-anodized TNT with diameter ranging from 25 to 100 nm, with the sweep potential in ranging from -1 to $+1$ V, measured in 0.01 M PBS solution. No anodic or cathodic peaks are observed on the CV graphs. It is extremely important

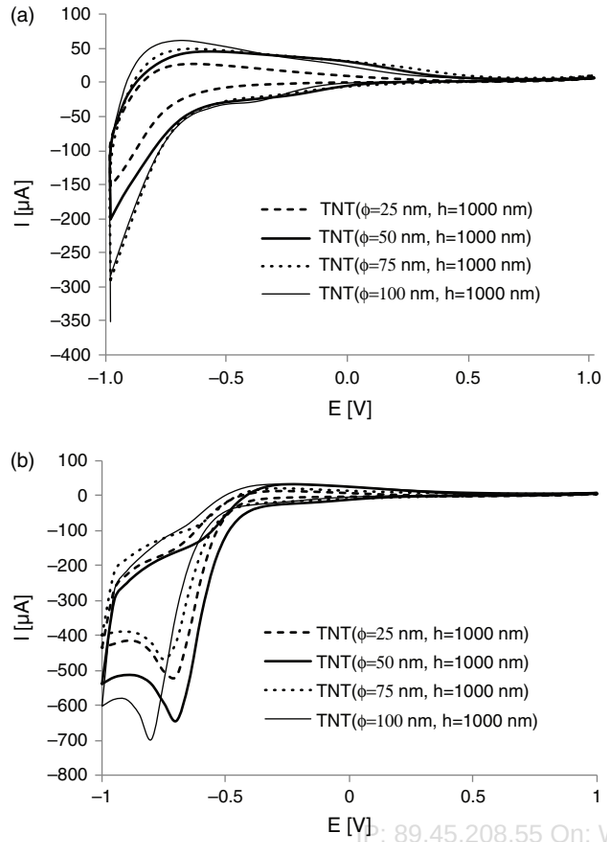

Figure 3. Cyclic voltammograms of TNT layers, 1000 nm thick (h) with nanotubes of diameters (ϕ): 25, 50, 75, 100 nm recorded in potential range $-1 \div 1$ V (vs. $E_{Ag/AgCl} = 0.222$ V), with scan rate 0.05 V/s in 0.01 M PBS (a) containing 1 mM potassium ferricyanide (b).

to use TNT layer as an electrochemical biosensor platform. The phenomena occurring at the metal-semiconductor boundary depend on the potential and space-charge layers near the semiconductor surface. Increased current values at approx. −0.8 V refer to the redox reaction: $Ti^{4+} + e \rightleftharpoons Ti^{3+}$. Kavan[60] suggests that it corresponds to the reduction of impurities, such as H_2O or O_2. It may also be caused by the accumulation layer on n-type semiconductor, which is characterized by an abundant number of charges (electrons) in the near-surface layer of TiO_2. Electrons moving up to the surface have higher energy and the TNT layer exhibits capacitive effect. Formation of the surface space charge region depleted by mobile charge carriers is related with rectangular potential barrier and bending of energy bands. The presence of an electron-rich layer at the surface of TNT confirms the electrical conductivity of formed layer.[28] Increasing values of current in the range $-1 \div -0.75$ V may also be caused by diffusion of ions in porous materials, what is confirmed by the difference between the cathodic and anodic current, which correlates with the diameter of TiO_2 nanotubes. The biggest difference was recorded for TNT with diameter of 100 nm and the smallest for 25 nm.

In order to determine the favorable biosensing properties of TiO_2 nanotube arrays, the amperometric detection of potassium ferricyanide was performed. This chemical compound is commonly used as an electron mediator in many amperometric biosensor. Figure 3(b) presents the cyclic voltammograms of ferri-ferrocyanide couple ($Fe(CN)_6^{3-}/Fe(CN)_6^{4-}$) obtained at non-annealed TiO_2 nanotubes with varying diameter values immersed in PBS solution (0.01 M, pH 7.4). Anodic and cathodic peaks are observed in every voltamogramms. Cathodic and anodic peak correspond to the formal oxidation–reduction potential of ($Fe(CN)_6^{3-}/Fe(CN)_6^{4-}$) ($E_o = -0.36$ V vs. hydrogen electrode[61]) taking into account the open circuit potential of TNT and the Ag/AgCl reference electrode potential ($E = 0.222$ V). TNT with diameters of 50 and 100 nm and 1000 nm thickness have exhibited the highest value of anodic potential peak.

Among the analized samples, the TiO_2 nanotubes (50 nm diameter and 1000 nm thickness) exhibit the most favorable biosensing properties, such as: reaching minimum value of impidance, adhesive hydrophilicity and the least resistance. Obtained results confirm and help to understand the measurements carried out by Oh[15] and Gongadze[14, 36] which indicate that the TNT layer with diameter 50 nm exhibit the ability to bind the protein and osteoblast.

3.2. Characterization of Thermal Modified TNT

Protein adsorption at solid surface in an aqueous environments is crucial for biosensor elaboration. When surfaces are charged, electrostatic interaction plays an important role because proteins are also charged (depending on the solution pH). Therefore, it is advisable to use thermal modification to improve the electrochemical and adsorption properties of on TNT layer. The TNT layers were annealed under different atmosphere: argon, nitrogen and air at 550 °C for 2 h. Annealing with inert (argon), reducing (nitrogen) or oxidizing (air) atmosphere intended to improve the electrical and optical properties by the anatase-rutile transformation.

Figure 4 shows the FE-SEM micrographs of TiO_2 nanotubes (1000 ± 100 nm thick, 50 ± 5 nm diameter) after thermal treatment by annealing in argon, nitrogen and air at 550 °C for 2 h. Obtained SEM images confirm that the thermal modification does not influence the homogeneity and morphology of TNT layers—its height and diameter have not been changed.

The results of EDS microanalysis for samples formed in ethylene glycol and thermally modified in argon, nitrogen and air are presented in Table III. The results show the difference in concentrations of elements in TiO_2 nanotube layer according to the formation conditions. After thermal treatment in every atmosphere, fluoride is not identified and the obtained titanium oxide is non-stoichiometric. Fluoride uptake caused an increase of oxygen content in

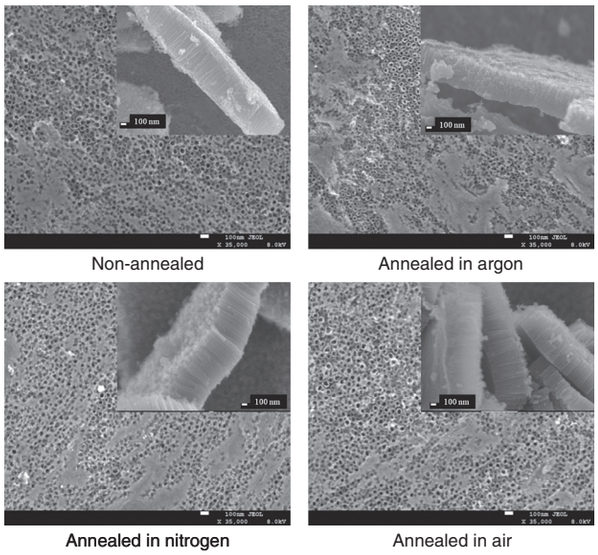

Figure 4. SEM top-view and cross-sectional images of TNT layers (50 nm diameter, 1000 nm thickness) annealed in argon, nitrogen or air atmosphere.

TNT annealed in argon (33.93%), nitrogen (32.80%) and air (34.82%). The highest amount of oxygen (34.82%) exhibit TNT layer annealed in air (oxygen source), which was enriched in this element after thermal modification. Annealing in argon could change the type of the ingredients of the oxide layer leading to the formation of oxygen vacancies. The possible explanation is due to tetravalent titanium Ti^{4+} to Ti^{3+} ions and the formation of oxygen vacancies.[62]

The results of the XPS analysis of the TNT layer (50 nm diameter and 1000 nm thick) annealed in varying atmosphere are shown in Figure 5. The presence of TiO_2 and Ti_2O_3 were confirmed for analyzed samples, both modified and non-modified TNT layer. The standard binding energy of Ti 2*p*3/2 in TiO_2 for Ti^{3+} is usually located at 457.7 eV and for Ti^{4+}-at 459.5 eV. The O 1*s* binding energy for TiO_2 is 529.3 eV.[63] Analysis of the XPS depth profile of a non-modified TNT layer indicates a higher amount of oxygen absorbed at the surface than inside of the oxide film. Thermal modification of the TNT in air caused the alignment of the oxygen amount in both layers. Surface enrichment of oxygen was found in samples of TNT layer annealed under nitrogen atmosphere. Similar intensity signals of

Table III. EDS investigation of TNT layer (50 nm diameter, 1000 nm thickness) before and after thermal modification (annealing in argon, nitrogen and air atmosphere in temperature 550 °C for 2 h).

[% wt.]	Annealed in argon	Annealed in nitrogen	Annealed in air	Non-annealed
Ti [%]	66.06	67.70	65.18	65.85
O [%]	33.93	32.80	34.82	25.59
F [%]				8.59

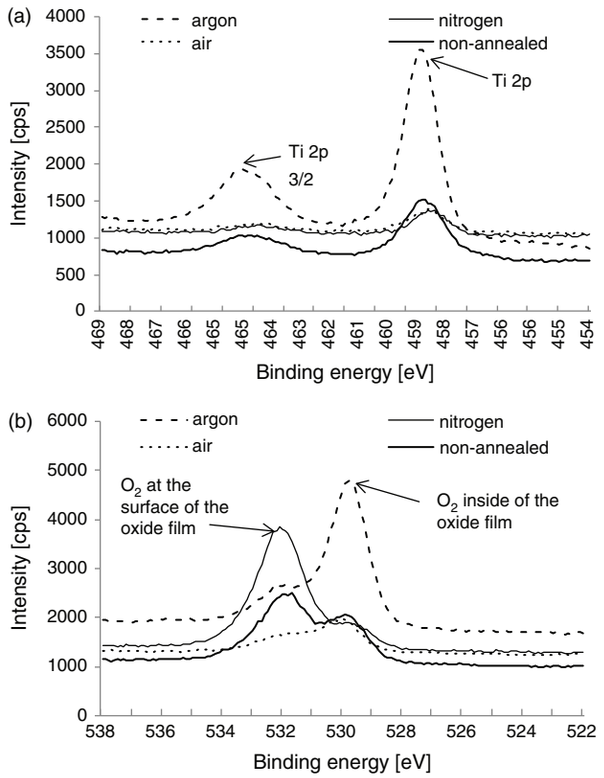

Figure 5. Chemical composition of a TNT surface (diameter 50 nm, 1000 nm thickness) before and after annealing in argon, nitrogen or air atmosphere in temperature 550 °C for 2 h measured with XPS (a) Ti 2*p* spectra, (b) O 1*s* spectra.

TiO_2 and Ti_2O_3 recorded for TNT annealed in nitrogen and air suggest that other compound than titanium oxides may occur on the surface of TNT annealed in nitrogen. Nitrogen atoms may be incorporated into the TNT layer during the anatase and/or rutile crystallization. TiN is unstable material which oxidise oxynitride at high temperature[62] what explains the large amount of oxygen TNT surface. Thermal modification of TNT under argon shows lack of oxygen in the surface, which proves its deficiency and the presence of oxygen vacancies.[64] The highest intensity of signals confirming the presence of TiO_2 titanium, Ti_2O_3, Ti^{3+} were also recorded for that samples, which is preferable for electric conductivity.

The results of contact angle and open circuit potential measurements for thermally modified TNT are presented in Table IV. The contact angle measurements carried out on the annealed samples for DI (doubly ionized) water, confirmed that all obtained surface layers are hydrophilic. The value of the contact angle for the non-annealed and annealed in nitrogen TiO_2 nanotubes, which amounts to $20° \pm 2°$, after annealing in air drops to 35°, whereas the corresponding values for samples thermally modified in argon are even quadruple. The materials with WCA around 90° are considered as hydrophobic/hydrophilic, which is favourable for

Table IV. Water contact angle (WCA) and open circuit potential (OCP) measurements of TNT layers (diameter 50 nm, 1000 nm thickness) before and after annealing in argon, nitrogen or air atmosphere in temperature 550 °C for 2 h.

TNT	WCA [°]	OCP [mV] versus Ag/AgCl
Annealed in argon	$80° \pm 5°$	55 ± 5
Annealed in nitrogen	$20° \pm 2°$	40 ± 5
Annealed in air	$35° \pm 3°$	-55 ± 10
Non-annealed	$20° \pm 2°$	-220 ± 10

immobilization process. Protein adsorption is stronger on the hydrophobic surface, but hydrophilic material helps to avoid the protein decomposition.[65] Annealing in argon also caused the increase of the open circuit potential value for Ti/TNT layers comparing to the stationary potential of non-annealed samples. Shift of the OPC potentials to more positive values is favourable for the immobilization of enzyme on the electrode surface. The basic aminoacid residues (e.g., HRP) and human antibodies exhibit negative charges in PBS (0.01 M, pH 7.4). The negatively charged protein molecules are easily pulled to the positive matrix of biosensor.[1]

The results of the EIS tests (Fig. 6) presented as Bode and Nyquist plots illustrate different impedance characteristics and corresponding structures of layers, which are dependent on thermal modification conditions.

Nyquist curves (Fig. 6(a)) recorded for the TNT layer annealed in varying atmospheres present fragments of large, incomplete semicircles. Additionally, the Warburg-type diffusion impedance were observed for the non-modified samples. The increase of the radius of semi-circle recorded for thermally modified TNT confirm increased electrolytic resistance of the electrolyte, which is associated with the presence of fluoride or with the interaction between the electrolyte and TNT layers. Bode plots (Fig. 6(b)) also confirms the influence of thermal modification on the properties of the TNT layer. Although different they reveal one, clearly defined, time constant in all impedance spectra which provides a single-layer structure of investigation samples. For treatment in air, the time constant within the higher frequency range (approx. 10^3 Hz) describe the capacitive character of the analyzed layer, whereas the other constant visible at a frequency of 1 Hz indicates the resistive nature of the TNT layer annealed in argon. The highest value of phase angle was measured for TNT annealed in argon, which means that this sample exhibits the highest homogeneity, a favorable properties for immobilization of biological materials on solid surface.

Cyclic voltammograms recorded for annealed and non-annealed TNT layer (Fig. 7(a)) in the PBS solution (pH 7.4) with the scan rate 0.05 V/s are flat, not showing any oxidation–reduction peaks in the potential ranging from -1 V to 1 V versus Ag/AgCl. This is a positive and required feature of material used as the biosensor

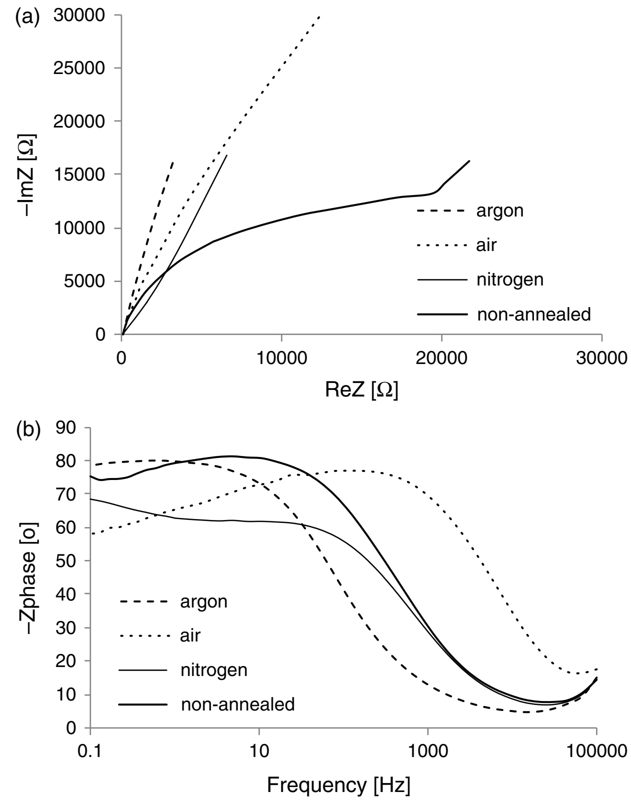

Figure 6. Nyquist (a) and Bode (b) plots of TNT layer (diameter: 50 nm and thickness: 1000 nm) before and after thermal modification—annealing in argon, nitrogen or air atmosphere in temperature 550 °C for 2 h. Spectra were recorded in the PBS solution (0.01 M, 10 ml, pH 7.4) over the frequency range 0.1–10^5 Hz with amplitude 10 mV versus $E_{Ag/AgCl} = 0.222$ V.

platform. The average anodic and cathodic current values, which are higher for samples modified in nitrogen may confirm their ionic affinity in PBS solution after thermal modification.

The amperometric detection of $K_3Fe(CN)_6$ by cyclic voltammetry for the TNT layer thermally modified under argon, nitrogen and air were shown in Figure 7(b). Having regard to Ag/AgCl electrode potential, formal redox potential of potassium ferricyanide ($E = -0.36$ V) and OPC potential of TNT thermally modified the shift of cathodic and anodic peak potential is observed. The electrochemical response signal of $K_3Fe(CN)_6$ is significantly enhanced at TNT with a diameter of 50 nm and a height of 1000 nm annealed in argon (Fig. 7(b), dashed line) which reflects the improvement of both the shape of redox peak and the magnitude of the peak current.

3.3. H_2O_2 Detection

The calibration curves for biosensor based on TNT layer as a platform in Figure 8 represented by a linear regression show that the prepared platform was sensitive to H_2O_2 in PBS solution. A limit detection of 3 μM of H_2O_2 was obtained with a good reproducibility for the developed

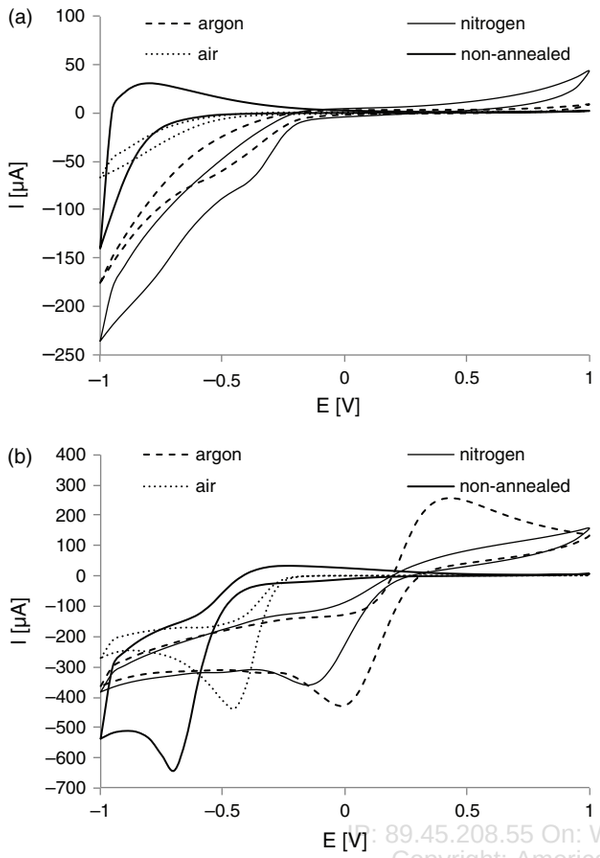

Figure 7. Cyclic voltammograms of TNT layers (diameter: 50 nm, thickness: 1000 nm) before and after thermal modification—annealing in argon, nitrogen or air atmosphere in temperature 550 °C for 2 h, recorded in potential range $-1 \div 1$ V (vs. $E_{Ag/AgCl} = 0.222$ V), with scan rate 0.05 V/s in 0.01 M PBS (a) containing 1 mM potassium ferricyanide (b).

biosensor. The biosensor response depends on the conductivity and the large surface-to-volume ratio attained with titania nanotubes and confirms the possibility of TNT layer exploitation in biosensors applications.

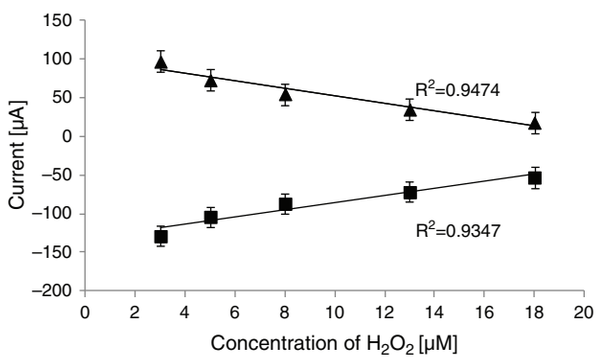

Figure 8. Cathodic (up triangle) and anodic (square) peaks for cyclic voltamperometry of TNT electrode measured in 0.01 M PBS containing 0.1 M HRP, varying concentration of H_2O_2 with scan rate 0.05 V/s.

4. CONCLUSIONS

Our study indicates that TiO_2 nanotubes reveals the favorable adsorption and electrical properties, which allow the direct immobilization of chemical substances on its surface. The effect of the morphology of the anodic layer on their electric and adsorption properties has been confirmed. The wettability, impedance character, stationary potential have been shown to correlate with the diameter and conditions of thermal modification of TiO_2 nanotubes. To maximize the response of potassium ferricyanide, an optimal TiO_2 nanotube diameter of 50 nm and 1000 nm-long, annealed in argon is required.

The performed analysis supplements another one described in literature, in which the optimal TNT diameter is 50 nm for protein binding,[14, 15, 36] explains the difference in wettability of TNT resulting from comparing TNT with varying diameter and hight simultaneously[56, 57] and defines the electrical conductivity of TNT dependent on rutile-anatase phase transformation through thermal modification in varying atmosphere.[62, 63] Obtained results are the explanation of physisorption mechanisms for TNT with the same height and different diameters, that was confirmed by potassium ferrocyanide and hydrogen peroxide detections.

The physicochemical characteristics of the titania nanotubes of the same height, which differs only in diameter, turned out to be a key and reasonable which substantially supplemented the existing literature reports.

Acknowledgment: The authors gratefully thank for the financial support received by the Ministry of Science and Higher Education in the Diamond Grant (No. DI2011 004941).

References and Notes

1. N. Sadana, Handbook of Biosensors and Biosensor Kinetics, edited by A. Sadana, Elsevier, Amsterdam **(2011)**.
2. C. Shan, H. Yang, D. Han, D. Han, Q. Zhang, A. Ivaska, and L. Niu, *Biosens. Bioelectron.* 25, 1070 **(2010)**.
3. R. Penu, A. C. Obreja, D. Patroi, M. Diaconu, and G. L. Radu, *Microchem. J.* 121, 130 **(2015)**.
4. S. Benítez-Martínez, Á. I. López-Lorente, and M. Valcárcel, *Microchem. J.* 121, 6 **(2015)**.
5. M. B. Gholivand and N. Karimian, *Sensors and Actuators B: Chemical* 215, 471 **(2015)**.
6. T. Rohani and M. Ali Taher, *Arabian Journal of Chemistry* 344, 1 **(2015)**.
7. H. Shekarchizadeh, A. A. Ensafi, and M. Kadivar, *Materials Science and Engineering: C* 33, 3553 **(2013)**.
8. Y. L. Wu, Q. W. Li, X. L. Zhang, X. Chen, and X. M. Wang, *Chin. Chem. Lett.* 24, 12 **(2013)**.
9. I. Roman, R. D. Trusca, M. L. Soare, C. Fratila, E. Krasicka-Cydzik, M. S. Stan, and A. Dinischiotu, *Materials Science and Engineering: C* 37, 374 **(2014)**.
10. M. Boehme, F. Voelklein, and W. Ensinger, *Sensors and Actuators B: Chemical* 158, 1 **(2011)**.
11. S. Baradaran, W. J. Basirun, E. Zalnezhad, M. Hamdi, A. D. Sarhanc, and Y. Alias, *Journal of the Mechanical Behavior of Biomedical Materials* 20, 272 **(2013)**.

12. H. Ch. Lee, L. F. Zhang, J. L. Lin, Y. L. Chin, and T. P. Sun, *Sensors* 13, 14161 (**2013**).

13. T. Kopac, K. Bozgeyik, and J. Yener, *Colloids and Surfaces A: Physicochemical and Engineering Aspects* 322, 19 (**2008**).

14. E. Gongadze, D. Kabaso, S. Bauer, P. Jung, P. Schmuki, and A. Iglic, *Mini Reviews in Medicinal Chemistry* 13, 194 (**2013**).

15. S. Oh, K. S. Brammer, Y. S. Li, D. Teng, A. Engler, S. Chien, and A. Jin, *Proceedings of the National Academy of Sciences of the United States of America* 106, 2130 (**2009**).

16. P. Xiao, Y. Zhang, and G. Cao, *Sensors and Actuators B: Chemical* 155, 159 (**2011**).

17. S. Oh, K. S. Brammer, K. S. Moon, J. M. Bae, and S. Jin, *Materials Science and Engineering: C, Materials for Biological Applications* 31, 873 (**2011**).

18. S. Oh, C. Daraio, L. H. Chen, T. R. Pisanic, R. R. Finones, and S. Jin, *Journal of Biomedical Materials Research, Part A* 78, 97 (**2006**).

19. J. Park, S. Bauer, K. von der Mark, and P. Schmuki, *Nano Lett.* 7, 1686 (**2007**).

20. J. Park, S. Bauer, P. Schmuki, and K. von der Mark, *Nano Lett.* 9, 3157 (**2009**).

21. S. Bauer, J. Park, J. Faltenbacher, S. Berger, K. von der Mark, and P. Schmuki, *Integrative Biology* 1, 525 (**2009**).

22. P. Roy, S. Bergen, and P. Schmuki, *Angewandte Chemie* 50, 2904 (**2011**).

23. J. M. Macak, H. Tsuchiya, L. Taveira, S. Aldabergerova, and P. Schmuki, *Angewandte Chemie* 117, 7629 (**2005**).

24. L. Y. Chin, Z. Zainal, M. Z. Hussein, and T. W. Tee, *J. Nanosci. Nanotechnol.* 11, 4900 (**2011**).

25. P. Acevedo, L. Lartundo-Rojas, and I. Gonzalez, *J. Solid State Electrochem.* 17, 2939 (**2013**).

26. A. Haring, A. Morris, and M. Hu, *Materials* 5, 1890 (**2012**).

27. A. R. Mohamed, N. Kasemphaibulsuk, S. Rohani, and S. Barghi, *J. Nanosci. Nanotechnol.* 10, 1998 (**2010**).

28. A. Kaczmarek, T. Klekiel, and E. Krasicka-Cydzik, *Surf. Interface Anal.* 42, 510 (**2003**).

29. R. Beranek, H. Hildebrand, and P. Schmuki, *Electrochem. Solid-State Lett.* 6, 12 (**2003**).

30. S. Yoriya, W. Kittimeteeworakul, and N. Punprasert, *Journal of Chemistry and Chemical Engineering* 6, 686 (**2012**).

31. V. Zwilling, M. Aucoutrier, and E. Dargue-Ceretti, *Electrochim. Acta* 45, 921 (**1999**).

32. E. Krasicka-Cydzik, K. Arkusz, and A. Kaczmarek, *Engineering of Biomaterials* 15, 34 (**2012**).

33. L. Giorgi, E. Salernitano, T. Dikonimos Makris, R. Giorgi, E. Leoni, M. L. Grilli, and N. Lisi, *Thin Solid Films* 601, 28 (**2016**).

34. C. Adán, J. Marugán, E. Sánchez, C. Pablos, and R. van Grieken, *Electrochim. Acta* 191, 521 (**2016**).

35. K. Arkusz, M. Nycz, E. Paradowska, and E. Krasicka-Cydzik, *Engineering of Biomaterials* 17, 21 (**2014**).

36. E. Gongadze, D. Kabaso, S. Bauer, T. Slivnik, and P. Schmuki, *International Journal of Nanomedicine* 6, 1801 (**2011**).

37. H. Yi-Hsien, K. Kuan-Chen, L. Tzer-Min, and W. Ching-Cheng, *Scientific Research and Essays* 6, 5750 (**2011**).

38. N. Wang, H. Li, W. Lü, J. Li, J. Wang, Z. Zhang, and Y. Liu, *Biomaterials* 32, 6900 (**2011**).

39. H. Li, Q. Cui, B. Feng, J. Wang, X. Lu, and J. Weng, *Appl. Surf. Sci.* 284, 179 (**2013**).

40. C. X. Cui, X. Gao, Y. M. Qi, S. J. Liu, and J. B. Sun, *Journal of the Mechanical Behavior of Biomedical Materials* 8, 178 (**2012**).

41. A. Shivaram, S. Bose, and A. Bandyopadhyay, *Journal of the Mechanical Behavior of Biomedical Materials* 59, 508 (**2016**).

42. M. S. AlHoshan, A. A. BaQais, M. I. Al-Hazza, and A. M. Al-Mayouf, *Electrochim. Acta* 62, 390 (**2012**).

43. T. Stergiopoulos, A. Ghicov, V. Likodimos, D. S. Tsouklevis, J. Kunze, P. Schmuki, and P. Falaros, *Nanotechnology* 19, 1143 (**2009**).

44. Y. K. Lai, J. Y. Huang, H. F. Zhang, V. P. Subramanian, Y. X. Tang, D. G. Gong, L. Sundor, L. Sun, Z. Chen, and C. J. Lin, *J. Hazard. Mater.* 184, 855 (**2010**).

45. C. Fabrega, T. Audreu, F. Guelle, J. D. Parades, S. Estrade, J. M. Redler, F. Peiro, and J. R. Morante, *Nanotechnology* 22, 2354 (**2011**).

46. F. Liu, L. Lu, P. Xiao, H. He, L. Qiao, and Y. Zhang, *Bull. Korean Chem. Soc.* 33, 72255 (**2012**).

47. A. Ghicov, H. Tsuchiya, J. M. Macak, and P. Schmuki, *Physica Status Solidi* 203, 28 (**2006**).

48. J. Wang and Z. Lin, *The Journal of Physical Chemistry C* 113, 4026 (**2009**).

49. K. N. Chappanda, Y. R. Smith, S. K. Mohanty, L. W. Rieth, P. Tathireddy, and M. Misra, *Nanoscale Research Letters* 7, 388 (**2012**).

50. J. M. Low, B. Curtain, M. Philipps, Z. Q. Liu, and M. Ionescu, *Journal of the Australian Ceramic Society* 48, 198 (**2011**).

51. Y. Wang, S. Liu, K. Huang, D. Fang, and S. Zhuang, *J. Solid State Electrochem.* 16, 723 (**2012**).

52. M. Salari, S. H. Aboutalebi, A. T. Chidembo, I. P. Nevirkovets, K. Konstantinov, and H. K. Liu, *PCCP* 14, 4770 (**2012**).

53. G. S. Zakharova, C. Jähne, A. Popa, C. Täschner, T. Gemming, A. Leonhardt, B. Büchner, and R. Klingeler, *The Journal of Physical Chemistry C* 116, 8714 (**2012**).

54. K. S. Han, D. K. Lee, J. W. Lee, G. I. Lee, and J. K. Kang, *Chemistry—A European Journal* 17, 2579 (**2011**).

55. D. Liu, P. Xiao, Y. Zhang, B. B. Garcia, Q. Zhang, Q. Guo, R. Champion, and G. Cao, *The Journal of Physical Chemistry C* 112, 11175 (**2008**).

56. Y. Q. Hao, S. J. Li, Y. L. Hao, Y. K. Zhao, and H. J. Ai, *Appl. Surf. Sci.* 268, 44 (**2013**).

57. Z. Lewandowska, P. Piszczek, A. Radtke, T. Jedrzejewski, W. Kozak, and B. Sadowska, *Journal of Materials Science: Materials in Medicine* 26, 163 (**2015**).

58. C. Liu, Y. Wang, M. Wang, W. Huang, and P. K. Chu, *Surf. Coat. Technol.* 206, 63 (**2011**).

59. W. Q. Yu, J. Qiu, and F. Q. Zhang, *Colloids and Surfaces B: Biointerfaces* 1, 400 (**2011**).

60. L. Kavan, M. Grätzel, J. Rathouský, and A. Zukal, *J. Electrochem. Soc.* 143, 394 (**1996**).

61. N. G. Tsierkezos, A. Knauer, and U. Ritter, *Thermochim. Acta* 576, 1 (**2014**).

62. V. G. Churpina, I. M. Shalya, and V. S. Zenkov, *Powder Metall. Met. Ceram.* 45, 82 (**2006**).

63. Y. G. Zhang, L. L. Ma, J. L. Li, and Y. Yu, *Environ. Sci. Technol.* 41, 6264 (**2007**).

64. M. A. Henderson, *Surf. Sci.* 419, 2 (**1999**).

65. G. Raffaini and F. Ganazzoli, *Journal of Applied Biomaterials and Biomechanics* 8, 135 (**2010**).

Received: 7 December 2016. Accepted: 20 April 2017.